

# High-Quality Exposure Correction of Underexposed Photos

Qing Zhang

Sun Yat-sen University

zhangqing.whu.cs@gmail.com

Ganzhao Yuan

Sun Yat-sen University

yuanganzhao@gmail.com

Chunxia Xiao

Wuhan University

cxxiao@whu.edu.cn

Lei Zhu

The Chinese University of Hong Kong

lzhu@cse.cuhk.edu.hk

Wei-Shi Zheng<sup>\*</sup><sup>†</sup>

Sun Yat-sen University

wszheng@ieee.org

## ABSTRACT

We address the problem of correcting the exposure of underexposed photos. Previous methods have tackled this problem from many different perspectives and achieved remarkable progress. However, they usually fail to produce natural-looking results due to the existence of visual artifacts such as color distortion, loss of detail, exposure inconsistency, etc. We find that the main reason why existing methods induce these artifacts is because they break a perceptually similarity between the input and output. Based on this observation, an effective criterion, termed as perceptually bidirectional similarity (PBS) is proposed. Based on this criterion and the Retinex theory, we cast the exposure correction problem as an illumination estimation optimization, where PBS is defined as three constraints for estimating illumination that can generate the desired result with even exposure, vivid color and clear textures. Qualitative and quantitative comparisons, and the user study demonstrate the superiority of our method over the state-of-the-art methods.

## CCS CONCEPTS

• Computing methodologies → Computational photography;

## KEYWORDS

Exposure correction; Illumination estimation; Perceptual similarity

### ACM Reference Format:

Qing Zhang, Ganzhao Yuan, Chunxia Xiao, Lei Zhu, and Wei-Shi Zheng. 2018. High-Quality Exposure Correction of Underexposed Photos. In *2018 ACM Multimedia Conference (MM '18), October 22–26, 2018, Seoul, Republic of Korea*. ACM, New York, NY, USA, 9 pages. <https://doi.org/10.1145/3240508.3240595>

## 1 INTRODUCTION

Exposure is one of the most important factors that determines whether the photographers can achieve the desired effect. For this

<sup>\*</sup>Corresponding author.

<sup>†</sup>Also with The Key Laboratory of Machine Intelligence and Advanced Computing, Ministry of Education (Sun Yat-sen University), Guangzhou, P.R. China..

Permission to make digital or hard copies of all or part of this work for personal or classroom use is granted without fee provided that copies are not made or distributed for profit or commercial advantage and that copies bear this notice and the full citation on the first page. Copyrights for components of this work owned by others than ACM must be honored. Abstracting with credit is permitted. To copy otherwise, or republish, to post on servers or to redistribute to lists, requires prior specific permission and/or a fee. Request permissions from permissions@acm.org.

MM '18, October 22–26, 2018, Seoul, Republic of Korea

© 2018 Association for Computing Machinery.

ACM ISBN 978-1-4503-5665-7/18/10...\$15.00

<https://doi.org/10.1145/3240508.3240595>

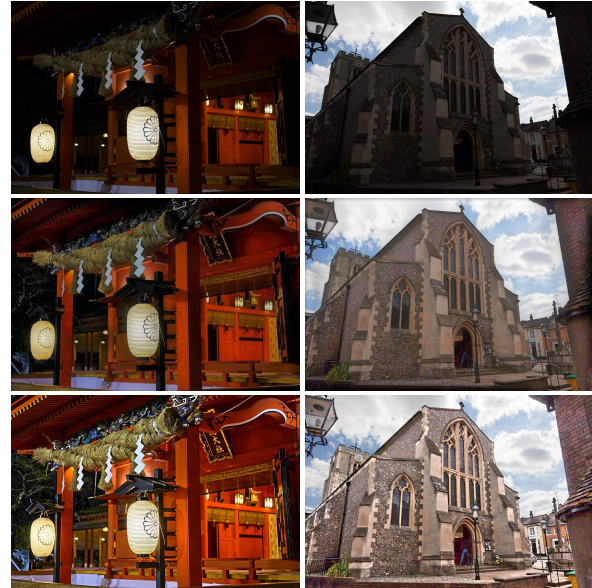


Figure 1: Top: two underexposed photos. Middle: results of the state-of-the-art [22]. Bottom: our results.

reason, most modern cameras are designed to allow exposure control. However, capturing well-exposed photos remains a challenge for non-expert users, since exposure is simultaneously determined by shutter speed, lens aperture and scene luminance, which are generally hard to control. As recording and sharing daily life in terms of photos has been evolved into a trendy lifestyle, lots of underexposed photos are inevitably created. Fig. 1 shows two examples. Basically, these images have barely invisible details and dull colors in underexposed regions, which severely limit their applicability for subsequent scenarios, e.g. Instagram and Facebook.

Many approaches have been developed for addressing this problem, which can be roughly classified into five main categories: histogram-based methods [5, 11, 19], S-curve based methods [1, 34], Retinex-based methods [9, 13, 31], fusion-based methods [8, 36] and learning-based methods [3, 22, 28]. Histogram-based methods are usually efficient, but may wash out details and induce oversaturated appearance. S-curve based methods rely on sigmoid mapping to adjust the exposure. They may incur uneven exposure or halo artifacts around the areas with abrupt exposure transition. Retinex-based methods work under the Retinex assumption [18] that an image can be decomposed into the product of reflectance and illumination. Although recent works in this category have

demonstrated impressive results, they typically suffer from a local overexposure issue. Fusion-based methods correct the exposure by fusing multiple inputs with different exposures into a single image. However, it will degrade the region contrast. Since learning-based methods are usually trained on synthesized images, they tend to produce unrealistic results.

In this paper, we propose a novel method for exposure correction of underexposed photos. Our main observation is that it is feasible to avoid the commonly encountered visual artifacts by preserving a visual similarity between the input and output. Based on this observation, we propose an effective criterion, called perceptually bidirectional similarity (PBS), for explicitly describing how to ensure the perceptual similarity between the two images. Then, we cast the exposure correction problem as a Retinex-based illumination estimation optimization, where we solve for the actual illumination of the input image under the constraint of PBS. With the estimated illumination, we obtain the final result based on the Retinex theory. We employ the ADMM technique [2] for optimizing the non-convex problem involved in our optimization model. Experiments on a number of challenging underexposed images and a user study demonstrate the advantage of our method over the state-of-the-art methods.

The main contributions of this paper are summarized as follows: (1) We propose PBS, an intuitive and effective criterion, that describes how to avoid the visual artifacts commonly encountered by previous methods. (2) We develop a PBS-constrained illumination estimation optimization model, which can produce high-quality exposure correction results for challenging underexposed photos. (3) We derive an ADMM based procedure for efficiently solving the proposed optimization model.

## 2 RELATED WORK

### 2.1 Histogram-based Methods

Histogram equalization (HE) [11] is one of the most widely adopted technique for exposure adjustment due to its simplicity. However, this technique may lead to loss of detail and appearance distortion, because it ignores the relationship between pixels. To address this issue, local HE methods [26, 39] are developed, but may distort the overall appearance. Celik et al. [5] proposed to enhance contrast by using a 2-D histogram based on the mutual relationship of spatially neighboring pixels. Lee et al. [19] further extended this work to multiple layers. Despite their effectiveness in contrast enhancement of normally exposed images, they typically fail to restore the underexposure.

### 2.2 S-curve based Methods

A well-known solution is Gamma correction. Similar to global HE based methods, it may also produce unsatisfying results. Bennett and McMillan [1] decomposed the input image into two layers by using bilateral filter [29], and then performed different S-curve mapping for each layer. The final result is obtained by recombined the two layers. This method can well preserve the details, but fails to maintain the global exposure consistency. Yuan and Sun [34] presented a region aware exposure correction method, where they segmented the input image into different subregions, and individually devised S-curve mapping for each subregion. However, it is



**Figure 2: Retinex theory and its relationship to exposure correction. Images from Grosse et al. [12].**

sensitive to the graph segmentation quality, and may not work well for challenging images with uneven exposure.

### 2.3 Retinex-based Methods

Jobson et al. [15, 16] made some early attempts, but their results are usually unrealistic. Wang et al. [31] presented a naturalness preserved algorithm by utilizing a lightness-order-error measure. However, it tends to produce results with dim details and requires expensive computational cost. Fu et al. [9] proposed a weighted variational model for simultaneously estimating reflectance and illumination. The limitation is that it may incur ghosting artifacts around regions with abrupt exposure transition. Guo et al. [13] estimated an initial illumination map, and refined it by only preserving the main contour. This method is effective in handling globally underexposed images, but may lead to overexposure issue for locally underexposed images. Our method also belongs to this category. In contrast, by maintaining PBS, we successfully avoid the visual artifacts encountered by previous methods.

### 2.4 Fusion-based Methods

The first framework is proposed by Mertens et al. [24] for reconstructing HDR image from multiple LDR images. Inspired by [24], Zhang et al. [36] constructed multi-exposure image sequence for the input image by sampling multiple S-curve mappings. They then progressively fused the image sequence with predefined perceptual metrics to produce the final result. Similarly, Fu et al. [8] derived multiple illumination maps based on both the Retinex theory and S-curve function. Thereafter, they obtained an adjusted illumination by blending advantages from different illumination maps, and computed the final result by compensating the adjusted illumination back to the reflectance. A common limitation of this kind of method is that they may degrade region contrast, and will produce unrealistic result for highly textured images.

### 2.5 Learning-based Methods

Bychkovsky et al. [3] proposed to learn global tone adjustment from expert retouched pairwise training images. However, this method is not designed for underexposed images, which differs our goal in essence. Lore et al. [22] presented a deep autoencoder for adaptively brightening underexposed images, but its advantage mainly lies in image denoising. Shen et al. [28] constructed MSR-net based on the multiscale Retinex theory and the feedforward convolution neural network. However, they may produce unrealistic results since their model is trained on synthesized pairwise images.

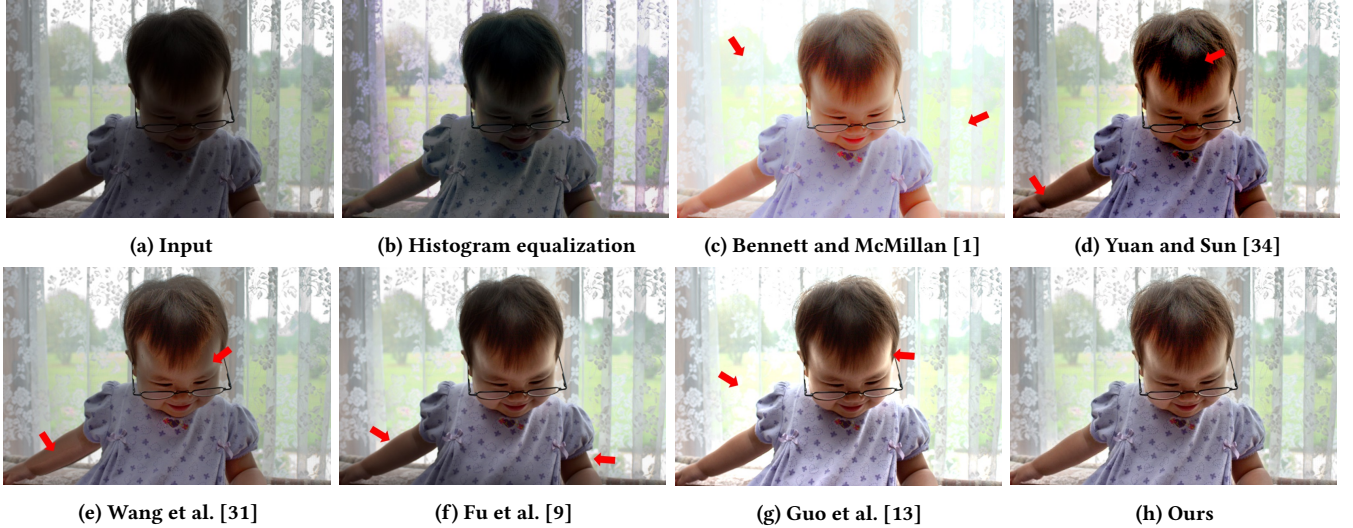


Figure 3: Issues encountered by previous methods. Photo from Bychkovsky et al. [3]. (Better view in electronic version).

### 3 OUR APPROACH

We first recall the Retinex theory [18], and analyze its relationship to exposure correction. Then, we introduce PBS and its mathematical description. Finally, we formulate the exposure correction problem as a PBS-constrained illumination estimation optimization, and describe an ADMM based procedure for solving the optimization.

#### 3.1 Retinex Theory

The Retinex theory assumes that an observed image  $I$  is the product of reflectance  $R$  and illumination  $S$ :

$$I = S \times R, \quad (1)$$

where  $S$  measures the amount of light reflected by the scene, and is determined by the light condition and the scene geometry.  $\times$  denotes pixel-wise multiplication.  $R$  represents the material RGB color that describes how objects reflect light, which is invariant to  $S$  and other imaging conditions. Note that, we in this paper assume that each color channel of  $R$  shares the same grayscale illumination.

In fact, exposure correction can be seen as a procedure for estimating the illumination independent reflectance, because it aims to remove the illumination effect and recover the original appearance of the scene objects. Fig. 2 validates this hypothesis, where the reflectance component exhibits a compelling exposure correction result for the original image. However, directly decomposing an input image into reflectance and illumination yields the intrinsic image decomposition problem [4, 7, 20, 27, 37, 38], which is inherently ill-posed and may produce unrealistic results [10, 13], because this problem is often built upon a reflectance smoothness prior not suitable for exposure correction. Thus, to simplify the problem while obtaining realistic results, we only estimate  $S$ , and then obtain the desired result by  $R = I/S$ , where the division is pixelwise.

#### 3.2 Perceptually Bidirectional Similarity

We begin by examining the issues encountered by previous methods in Fig. 3. As shown, color distortions, loss of details and exposure inconsistency are three main issues. Our observation is that the

main reason why these results are not satisfactory is because they are not consistent to the input. For example, Wang et al. [31] turn the girl's face and arms to gray, which leads to loss of their underlying color and introduction of mismatched color. Bennett and McMillan [1] and Guo et al. [13] overexpose the background and degrade the textures. Result of Yuan and Sun [34] and Fu et al. [9] exhibit clear exposure inconsistencies around the arms and the body, while these regions have consistent exposure in the input.

To remove the issues encountered by existing methods, we propose to ensure the visual consistency between the input and output by preserving a perceptual similarity criterion, namely PBS. Formally, we define PBS as the following two requirements between the input  $I$  and the expected result  $R$ :

- All colors and textures in  $I$  should exist in  $R$ , and appear as properly enlarged version. Regions have consistent exposure in  $I$  should also have consistent exposure in  $R$ .
- $R$  should not contain colors, textures or exposure inconsistency that originally do not exist in  $I$ .

To utilize PBS, we convert it into specific numerical constraints on color, texture and exposure below.

**Color Consistency Constraint.** Suppose the input image  $I$  is normalized to  $[0,1]$ . Since  $R = I/S$ , smaller  $S$  will produce  $R$  with higher RGB values, and larger  $S$  corresponds to  $R$  with lower RGB values. The upper bound of  $S$  is 1, in which case the input will be directly taken as the output. Intuitively, the color inconsistency will happen when  $S$  is too small to ensure that each color channel of estimated  $R$  are within the normal color gamut  $[0,1]$ . As a result, unpredictable colors will be introduced due to naive color truncation. To avoid this issue, we constrain the illumination at each pixel no less than the value that can just enlarge the maximum color channel of  $I$  to 1. Mathematically, we have

$$\max I_p^c = \Gamma(S_p^{\min}), \quad c \in \{r, g, b\}, \quad (2)$$

where  $I_p^c$  is a color channel at pixel  $p$ .  $\Gamma(\cdot)$  is the gamma function  $\Gamma(\alpha) = \alpha^\gamma$  with  $\gamma \in (0, 1)$ , which is an optional operation used for further illumination adjustment. Based on Eqn. 2, we have



**Figure 4: An example backlit photo restored by our method.** (a) Input. (b) Initial illumination  $S'$ . (c) Result computed from  $S'$ . (d) Our estimated illumination  $S$ . (e) Our result from  $S$ . Note the grayscale illuminations are visualized using the jet colormap.

$S_p^{\min} = (\max I_p^c)^{1/\gamma}$ . The color consistency constraint can then be characterized as  $S_p^{\min} \leq S_p \leq 1$ .

**Texture Consistency Constraint.** To ensure texture consistency, we reformulate PBS from a viewpoint of edge consistency as follows: (1) If  $I$  is smooth at pixel  $p$ , then  $R$  should also be smooth at  $p$ ; (2) If  $I$  has an edge at pixel  $p$ , then  $R$  should have a stronger, or at least equivalent edge at  $p$ . By associating edge with gradient and directional derivatives, above two cases can be defined by:

$$\begin{cases} \nabla R_p = 0, & |\nabla I_p| \leq \tau \\ \partial_d R_p / \partial_d I_p \geq 1, & |\nabla I_p| > \tau \end{cases} \quad (3)$$

where  $\nabla$  denotes the gradient operator.  $\partial_{d \in \{x, y\}}$  denotes the first order derivative along the horizontal and vertical.  $\tau$  is a small constant (typically 1e-5) used for determining whether there is an edge at a pixel in the input image  $I$ . In general, small  $\tau$  can better preserve textures, while large  $\tau$  may lead to loss of textures. Eqn. 3 can also be expressed in terms of  $S$  by replacing  $R$  with  $I/S$ .

**Exposure Consistency Constraint.** Illumination distribution essentially determines whether an image has consistent exposure. According to the Retinex theory, the key to preserving the exposure consistency in  $R$  is to ensure that illumination  $S$  is piecewise smooth, which also complies with the illumination distribution in natural images and can help to recover clear details from underexposed regions. In what follows, we will introduce how we use a total variation measure to obtain piecewise smooth  $S$ .

### 3.3 Illumination Estimation Optimization

The input image actually reflects the coarse illumination distribution. Inspired by [18], we obtain an initial illumination  $S'$  by  $S'_p = \max I_p^c$ . The reason why we choose the maximum values among the RGB channels is that this setting can avoid sending color channels out of the color gamut when performing  $R_p = I_p^c / S'_p$ .

With the initial illumination and the PBS constraints, we define the following framework for estimating the ideally illumination that can produce high-quality results free of aforementioned issues:

$$\arg \min_S E(S) = E_d(S) + \lambda_c E_c(S) + \lambda_t E_t(S) + \lambda_e E_e(S), \quad (4)$$

where  $E_d$  denotes the data term that enforces  $S$  to be similar with  $S'$ .  $E_c$ ,  $E_t$  and  $E_e$  denote the PBS constraints on color, texture and exposure.  $\lambda_c$ ,  $\lambda_t$  and  $\lambda_e$  are balancing weights.

Inspired by previous Retinex algorithms [7, 17, 25, 30], which have demonstrated that total variation has good performance in promoting illumination smoothness, we alternatively adopt the relative total variation (RTV) introduced by Xu et al. [32] for obtaining

piecewise smooth  $S$ . It is worth mentioning that any other smoothness regularizer can also work with our framework. By replacing the energy terms in Eqn. 4 with specific formulations, the objective function can be expressed as follows:

$$\begin{aligned} \arg \min_S & \sum_p (S_p - S'_p)^2 + \lambda (\mathcal{H}(S_p) + \mathcal{V}(S_p)), \\ \text{s.t. } & S_p^{\min} \leq S_p \leq 1, \quad \begin{cases} \nabla(I_p / S_p) = 0, & |\nabla I_p| \leq \tau \\ \partial_d(I_p / S_p) / \partial_d I_p \geq 1, & |\nabla I_p| > \tau \end{cases} \end{aligned} \quad (5)$$

where  $\mathcal{H}(S_p)$  and  $\mathcal{V}(S_p)$  denote the horizontal and vertical relative total variation (RTV) measure.  $\lambda$  is a weight.

### 3.4 Solver

The objective function in Eqn. 5 involves a non-convex problem. To obtain its solution, we develop an efficient solver based on the ADMM technique [2]. Before describing the details, we first transform the Retinex theory in Eqn. 1 to log-domain, so that we can reduce the nonlinear operation on  $S$  in Eqn. 3 to linear form.

Let  $\mathcal{I} = \log(I)$ ,  $\mathcal{R} = \log(R)$ ,  $\mathcal{S} = \log(S)$  and  $\mathcal{S}' = \log(S')$ , we then have  $\mathcal{I} = \mathcal{R} + \mathcal{S}$ . The color and texture constraints can be accordingly expressed as  $S_p^{\min} \leq S_p \leq 1$  and

$$\begin{cases} \nabla(\mathcal{I} - \mathcal{S})_p = 0, & |\nabla I_p| \leq \tau \\ e^{\mathcal{I} - \mathcal{S}} \partial_d(\mathcal{I} - \mathcal{S})_p / (e^{\mathcal{I}} \partial_d I_p) \geq 1, & |\nabla I_p| > \tau \end{cases} \quad (6)$$

As  $\frac{\partial(\log(v))}{\partial x} = \frac{1}{v} \frac{\partial v}{\partial x}$ , similar to [9], we multiply by  $R = e^{\mathcal{I} - \mathcal{S}}$  and  $I = e^{\mathcal{I}}$  on both sides of the second line of Eqn. 6 to eliminate the impact of  $\frac{1}{v}$ . Note that  $R$  can be estimated from previous iteration and seen as constant during the optimization.

According to analysis in [32],  $\mathcal{H}(S_p)$  can be written as:

$$\mathcal{H}(S_p) = \sum_{q \in N_p} u_q^x w_q^x (\partial_x S_q)^2, \quad (7)$$

where  $u_q^x = G_\sigma * (|G_\sigma * \partial_x S_q| + \epsilon)^{-1}$  and  $w_q^x = (|\partial_x S_q| + \epsilon)^{-1}$ .  $G_\sigma$  denotes the Gaussian smoothing with standard deviation  $\sigma = 3$ .  $*$  denotes the convolution operator.  $\mathcal{V}(S_p)$  is defined similarly. With above transformation, the main body of the objective function in Eqn. 5 can be further written in a matrix form:

$$\begin{aligned} \|\mathbf{S} - \mathbf{S}'\|_F^2 + \lambda (\mathbf{S}^T \mathbf{D}_x^T \mathbf{H}_x \mathbf{D}_x \mathbf{S} + \mathbf{S}^T \mathbf{D}_y^T \mathbf{H}_y \mathbf{D}_y \mathbf{S}), \\ \text{s.t. } \mathbf{S}^{\min} \leq \mathbf{S} \leq 0, \quad \begin{cases} \nabla(\mathbf{I} - \mathbf{S}) = 0, & \mathbf{M}_p = 0 \\ \mathbf{C}_d \mathbf{D}_d (\mathbf{I} - \mathbf{S}) \geq 1, & \mathbf{M}_p = 1 \end{cases} \end{aligned} \quad (8)$$

where  $\mathbf{S}$ ,  $\mathbf{S}'$  and  $\mathbf{I}$  are vector representation of  $S$ ,  $S'$  and  $I$ .  $\mathbf{H}_x$  and  $\mathbf{H}_y$  are diagonal matrices with values  $\mathbf{H}_x[i, i] = u_i^x w_i^x$ ,  $\mathbf{H}_y[i, i] =$

---

**Algorithm 1** Illumination Estimation Optimization

---

**Input:** Input image  $I$ , initial illumination  $S'$ , parameter  $\lambda$

- 1: **Initialization:** Set  $Z, X, Y, \xi, \zeta, \pi$  as zero matrices. Set  $k = 1, \beta, \eta > 0$
- 2: **while** not converged **do**
- 3: Solve  $S_{k+1}$  in Eqn. 11a
- 4: Solve  $Z_{k+1}, X_{k+1}$  and  $Y_{k+1}$  in Eqn. 12
- 5: Update  $\xi_{k+1}, \zeta_{k+1}$  and  $\pi_{k+1}$  in Eqn. 13
- 6:  $\beta = \eta\beta$  and  $k = k + 1$
- 7: **end while**

**Output:** The estimated illumination  $S$

---

$u_i^y w_i^y$ .  $D_x$  and  $D_y$  are the Toeplitz matrices from the discrete gradient operators with forward difference.  $M$  is a binary matrix indicating whether a pixel  $p$  satisfies  $|\nabla I_p| > \tau$ .  $C_x$  and  $C_y$  are diagonal matrices consisting of constant parts in Eqn. 6.

To apply ADMM, we reformulate the problem in Eqn. 8 as the following equivalent form:

$$\begin{aligned} \min_S \|S - S'\|_F^2 + \lambda \left( S^T W_x S + S^T W_y S \right) \\ \text{s.t. } \mathcal{J}(S) = Z, \mathcal{F}^x(S) = X, \mathcal{F}^y(S) = Y, \\ Z = 0, X \geq 1, Y \geq 1, S^{\min} \leq S \leq 0, \end{aligned} \quad (9)$$

where  $W_x = D_x^T H_x D_x$ ,  $\mathcal{J}(S) = \nabla(I - S)$  and  $\mathcal{F}^x(S) = C_x D_x(I - S)$ .  $W_y$  and  $\mathcal{F}^y(S)$  are defined similarly.  $Z, X$  and  $Y$  are auxiliary variables for making the original problem separable. The augmented Lagrangian function of Eqn. 9 is:

$$\begin{aligned} \mathcal{L}(S, Z, X, Y, \xi, \zeta, \pi) = & \|S - S'\|_F^2 + \lambda S^T W_x S \\ & + \lambda S^T W_y S + \langle \xi, Z - \mathcal{J}(S) \rangle + \beta \|Z - \mathcal{J}(S)\|_F^2 \\ & + \langle \zeta, X - \mathcal{F}^x(S) \rangle + \beta \|X - \mathcal{F}^x(S)\|_F^2 \\ & + \langle \pi, Y - \mathcal{F}^y(S) \rangle + \beta \|Y - \mathcal{F}^y(S)\|_F^2, \end{aligned} \quad (10)$$

where  $\xi, \zeta$  and  $\pi$  are Lagrangian multipliers,  $\beta$  is the penalty parameter.  $\langle \cdot \rangle$  computes the standard trace inner product.

The problem in Eqn. 10 can be further divided into following subproblems with respect to  $S, Z, X$  and  $Y$ :

$$S_{k+1} = \arg \min_{S^{\min} \leq S \leq 0} \mathcal{L}(S, Z_k, X_k, Y_k, \xi_k, \zeta_k, \pi_k), \quad (11a)$$

$$Z_{k+1} = \arg \min_{Z=0} \mathcal{L}(S_{k+1}, Z, X_k, Y_k, \xi_k, \zeta_k, \pi_k), \quad (11b)$$

$$X_{k+1} = \arg \min_{X \geq 1} \mathcal{L}(S_{k+1}, Z_{k+1}, X, Y_k, \xi_k, \zeta_k, \pi_k), \quad (11c)$$

$$Y_{k+1} = \arg \min_{Y \geq 1} \mathcal{L}(S_{k+1}, Z_{k+1}, X_{k+1}, Y, \xi_k, \zeta_k, \pi_k), \quad (11d)$$

where  $k$  denotes the  $k$ th iteration. By iteratively solving subproblems one at a time while fixing others at their most recent values until convergence, we can obtain the solution to Eqn. 9. Specifically, we first obtain  $S_{k+1}$  by solving the subproblem in Eqn. 11a. With  $S_{k+1}$ , we then compute  $Z_{k+1}, X_{k+1}$  and  $Y_{k+1}$  by:

$$\begin{aligned} Z_{k+1} &= \mathcal{P}_0(\mathcal{J}_{k+1}(S_{k+1}) - \xi_k / \beta), \\ X_{k+1} &= \mathcal{P}_1(\mathcal{F}_{k+1}^x(S_{k+1}) - \zeta_k / \beta), \\ Y_{k+1} &= \mathcal{P}_1(\mathcal{F}_{k+1}^y(S_{k+1}) - \pi_k / \beta), \end{aligned} \quad (12)$$

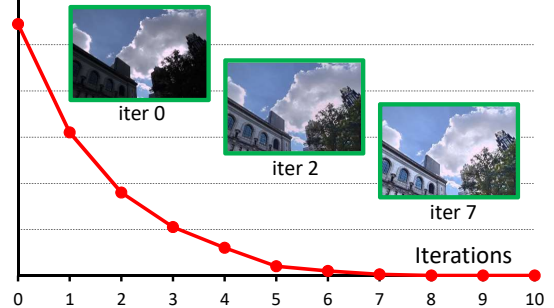


Figure 5: Convergence curve of our algorithm. The ordinate axis indicates the iterative error of the solution.

where  $\mathcal{P}_0(\cdot)$  projects entries that satisfy  $M_p = 0$  to zero.  $\mathcal{P}_1(\cdot)$  ensures that other entries ( $M_p \neq 0$ ) are no less than 1. The Lagrangian multipliers are updated by:

$$\begin{aligned} \xi_{k+1} &= \xi_k + \eta\beta(Z - \mathcal{J}_{k+1}(S_{k+1})), \\ \zeta_{k+1} &= \zeta_k + \eta\beta(X - \mathcal{F}_{k+1}^x(S_{k+1})), \\ \pi_{k+1} &= \pi_k + \eta\beta(Y - \mathcal{F}_{k+1}^y(S_{k+1})), \end{aligned} \quad (13)$$

where  $\eta \in (0, 2)$  is the relaxation parameter. The whole ADMM procedure for our approach is summarized in Algorithm 1.

### 3.5 Implementation and Parameter Settings

We use projected gradient descent method [21] for solving the subproblem in Eqn. 11a. The range constraint such as  $S^{\min} \leq S \leq 0$  can be accordingly ensured by a projection operation. The key parameter of our approach is  $\lambda$ , which determines the smoothness level of the illumination  $S$ . In general, we use larger  $\lambda$  for highly textured images.  $\gamma$  is another parameter that affects the result quality. In all our experiments, we set  $\lambda = 0.8$  and  $\gamma = 0.6$ . The final result is obtained by  $R = I/S^Y$ . Fig. 4 shows an example.

The convergence condition of Algorithm. 1 is: (i) the difference between two consecutive solutions are no more than a small constant (10e-5), or (ii) the maximum number (we empirically set it as 20) of iterations is reached. We have experimentally found that our algorithm has good convergence rate when  $\beta = 1$  and  $\eta = 1.9$ , and usually converges in 5-10 iterations. Fig. 5 plots the convergence curve of our algorithm for an example image.

## 4 EXPERIMENT

In this section, we present experiments to evaluate the performance of our method. We first demonstrate our advantage over state-of-the-art methods [6, 8, 13, 22, 31, 34] by qualitative and quantitative comparisons, and a user study. The testing datasets are NPE dataset [31], MEF dataset [23, 35], MF dataset [8], LIME dataset [13] and the VV dataset<sup>1</sup>. It is worth noting that we implement [34] by ourselves. While codes of other comparative methods are obtained from the author's websites. Then, we perform evaluation of the proposed method by conducting one-by-one evaluation of the PBS constraints, and analyzing the effect of different parameter settings, the time complexity and its limitations. All the experiments are carried out on a PC with Intel Core i5-7400 CPU using Matlab. Our code is available at: <http://isee.sysu.edu.cn/~zhangqing/>.

<sup>1</sup><https://sites.google.com/site/vonikakis/datasets>

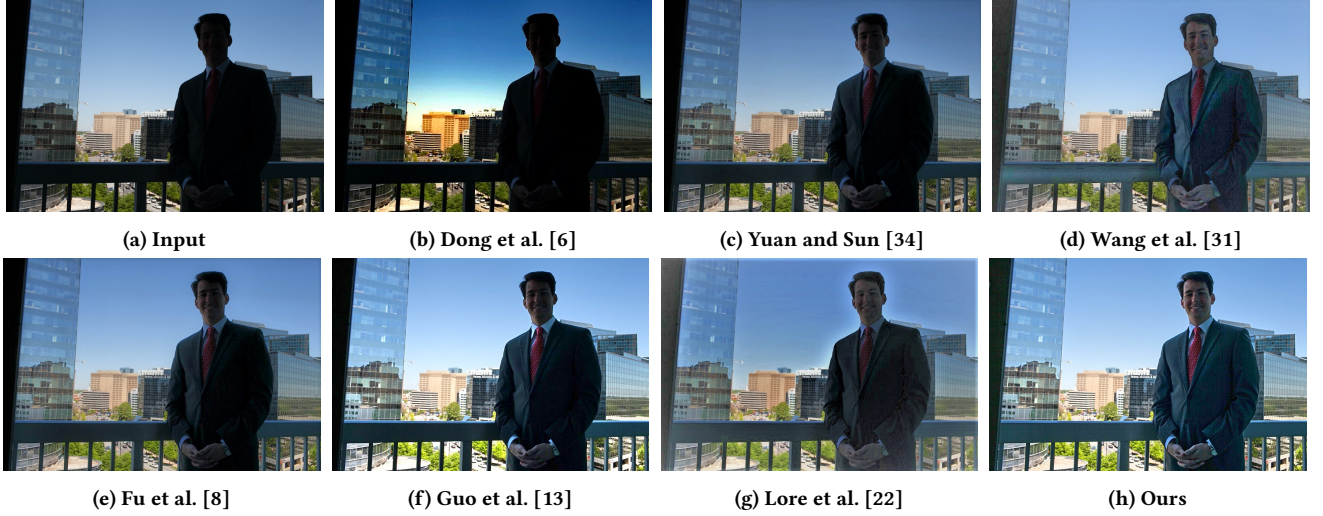


Figure 6: Comparison with state-of-the-art methods on the image “*Man*”. (Better view in electronic version).

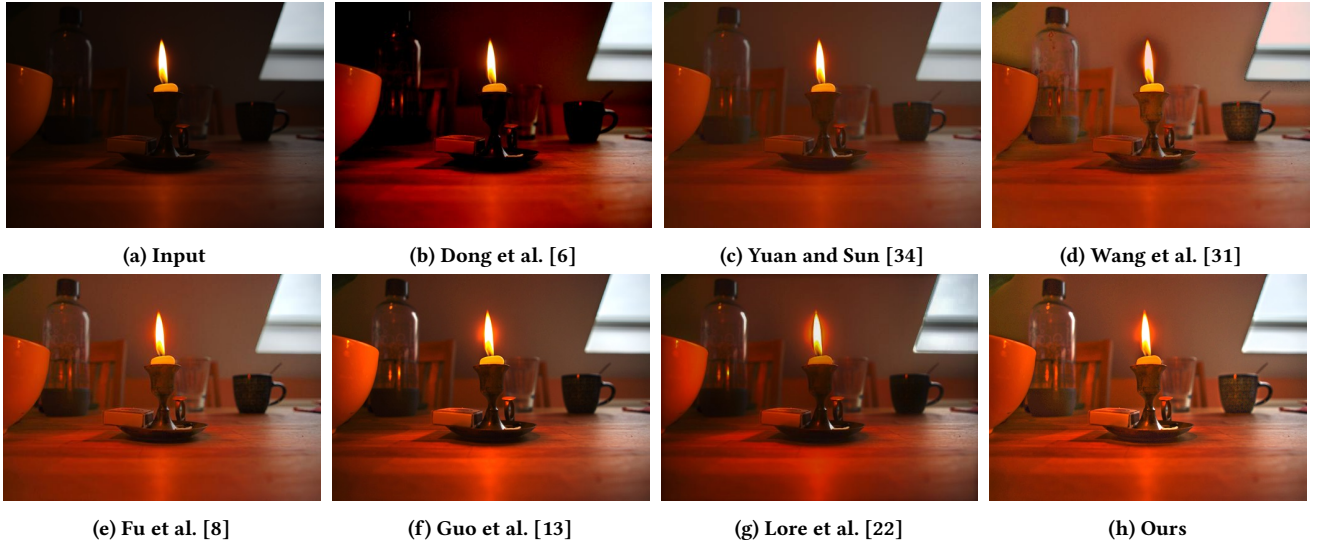


Figure 7: Comparison with state-of-the-art methods on the image “*Candle*”. (Better view in electronic version).

#### 4.1 Comparison with State-of-the-Art Methods

Here, we demonstrate the advantage of our method over the state-of-the-art methods in terms of both qualitative and quantitative comparisons, and a user study.

**Qualitative Comparisons.** Fig. 6 examines the performance of different methods in handling a challenging backlit photo with severely underexposed foreground. [6] enhances the background, but makes the foreground even more underexposed. [34] improves the underexposure. However, compared with the background, the foreground is still underexposed, and lots of details are still barely invisible. [31] restores the foreground, but induces clear color distortions. Similar to [34], [8] also cannot recover all hidden details from the underexposure. [13] is effective in enhancing the local contrast. However, it fails to ensure exposure consistency. As a result, the left part of the person is darker than the right part, which makes the result somewhat unnatural. Result of [22] is unrealistic due to the

distorted appearance and halo artifacts. In contrast, our method successfully lights up the foreground, and obtains high-quality result. Another comparison is conducted on an indoor image captured under low light condition in Fig. 7. As shown, our method avoids artifacts such as color distortions and exposure inconsistencies. Moreover, it restores the exposure for the candlestick and mug, which is not enabled by most comparative methods.

**Quantitative Comparisons.** Similar to previous methods [8], we adopt two commonly used no reference image quality assessment metrics, namely discrete entropy (DE) [33] and natural image quality evaluator (NIQE) [14] for quantitative evaluation. DE measures the performance of detail enhancement. NIQE assesses the overall naturalness of the result. In general, higher DE means that details or visibility are better enhanced, while lower NIQE indicates higher overall naturalness. Table 1 shows the quantitative comparisons on datasets. The original average DE and NIQE values

**Table 1: Comparison of average DE and NIQE on five datasets.**

Dataset	Original		Dong et al. [6]		Yuan and Sun [34]		Wang et al. [31]		Fu et al. [8]		Guo et al. [13]		Lore et al. [22]		Ours	
	DE	NIQE	DE	NIQE	DE	NIQE	DE	NIQE	De	NIQE	DE	NIQE	DE	NIQE	DE	NIQE
NPE	6.563	3.895	6.841	3.639	7.135	3.412	7.221	3.182	7.376	3.309	7.539	3.443	7.434	3.483	<b>7.643</b>	<b>3.021</b>
MEF	6.071	4.277	6.658	3.945	7.108	3.751	7.142	3.586	7.244	3.613	7.321	3.701	7.237	3.861	<b>7.561</b>	<b>3.372</b>
MF	6.365	3.357	6.937	3.362	7.042	3.196	7.113	3.017	7.345	3.167	7.499	3.122	7.431	3.149	<b>7.739</b>	<b>2.813</b>
LIME	6.025	4.478	6.557	4.315	6.725	4.186	6.904	4.096	7.076	4.067	7.389	4.102	7.214	4.213	<b>7.452</b>	<b>3.569</b>
VV	6.638	3.382	7.214	3.279	7.389	2.877	7.427	<b>2.732</b>	7.436	2.793	7.529	2.895	7.367	2.972	<b>7.812</b>	2.746

■ Dong et al. ■ Yuan and Sun ■ Wang et al. ■ Fu et al. ■ Guo et al. ■ Lore et al. ■ Ours

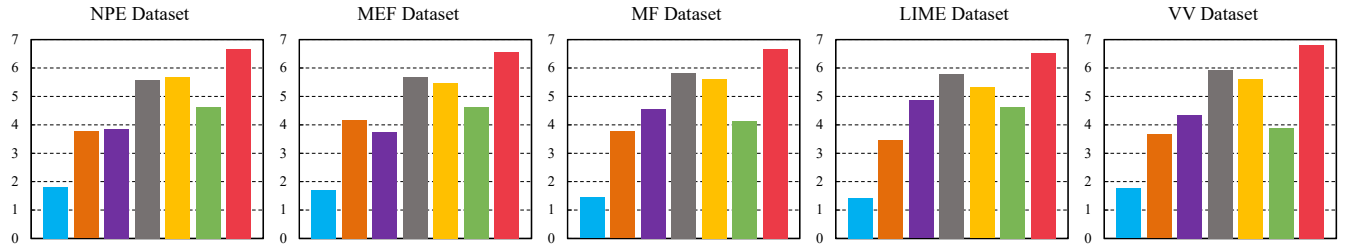


**Figure 8: User study. We show the average points obtained by each method on different datasets.**

for different datasets are also shown for reference. As shown, all methods increase DE through contrast enhancement, and reduce the NIQE because of lightening the underexposed regions. Our method achieves higher DE and lower NIQE than other methods on almost all the datasets. The reason why we obtain better results is twofold: (1) Our method can effectively recover and enlarge the barely invisible details due to the merit of the texture and exposure consistency constraints; (2) We can avoid the visual artifacts commonly encountered by previous method.

**User Study.** We performed a user study on the five datasets (106 images in total) to demonstrate that our method can generate visually more appealing results than state-of-the-art methods [6, 8, 13, 22, 31, 34]. The detailed procedure is introduced below.

We invited 30 subjects to rank their preferences to results of different methods. For each input image, each subject was asked to rate 7 results (ours and other 6 comparative methods) using 1 (least favorite) to 7 points (most favorite), according to the following 4 requirements for the desired result : (1) clear details in originally underexposed regions, (2) no loss of details, (3) no color distortions, (4) no exposure inconsistencies. To avoid the subjective bias, subjects were assigned with anonymous results in random orders. In addition, the user study was conducted in the same environment (room, light and monitor). After the subjects finished rating all the results, we computed the average points obtained by each method on different datasets. We summarize the user study results in Fig. 8. As can be seen, results generated by our algorithm are more preferred by human subjects in average.

## 4.2 Evaluation of the proposed Method

We first validate the effectiveness of the proposed PBS constraints. Then, we analyze how  $\lambda$  and  $\gamma$  affect the result. Finally, we introduce the time complexity and the main limitations of our method.

**Validation of PBS Constraints.** As shown in Fig. 9, without the color consistency constraint, the right side of the boy’s face exhibits clear color distortion. The textures on the curtain are severely

degraded without the texture constraint. Without the exposure constraint, we fail to generate result with smooth exposure and clear details. In contrast, we obtain a high-quality result by combining all the three PBS constraints. Since we employ Gamma function for post processing, we compare with it for illustrating the difference. In addition, we show result directly computed from the initial illumination  $S'$ , which is used as a baseline. Our illumination estimation optimization essentially involves a smoothing procedure to the initial illumination, which is akin to the original RTV method [32]. As we use RTV in our model, we also compare with the result derived from [32]. As shown, our method produces more realistic result with consistent exposure and clear details, while result of RTV method has overexposed appearance.

**Effect of varying  $\lambda$  and  $\gamma$ .** Fig. 10 evaluates the effect of varying  $\lambda$ . As shown, larger  $\lambda$  produces result with stronger local contrast. However, this effect becomes less obvious when  $\lambda > 0.8$ . As larger  $\lambda$  typically requires more iterations to converge, we fix  $\lambda = 0.8$  as a trade-off. Fig. 11 shows how the Gamma function affects the final result. We can see that result without Gamma function (namely  $\gamma = 1$ ) is also satisfactory, but too bright to be consistent with the image aesthetics. Decreasing  $\gamma$  can reduce the overall brightness, but at the cost of lowering the visibility. To obtain better visual results, we set  $\gamma = 0.6$  for all our tested images.

**Time Complexity.** Our method takes about 3 seconds to process a  $800 \times 1200$  image, which is slightly slower than [8] and [13]. However, our current Matlab implementation is neither optimized nor accelerated. By using more efficient solvers for the subproblem in Eqn. 11a and the GPU parallelization, our method can be sped up to provide nearly instant feedback for consumer photographs.

**Limitations.** As shown in Fig. 12, our method induces disturbing blocking artifacts for regions that are nearly pure black (most color channels are close or equal to 0). Another limitation is that our method will enlarge noise. In the future, we will explore the possibility of leveraging deep learning to handle pure black regions, and simultaneously remove the noise.

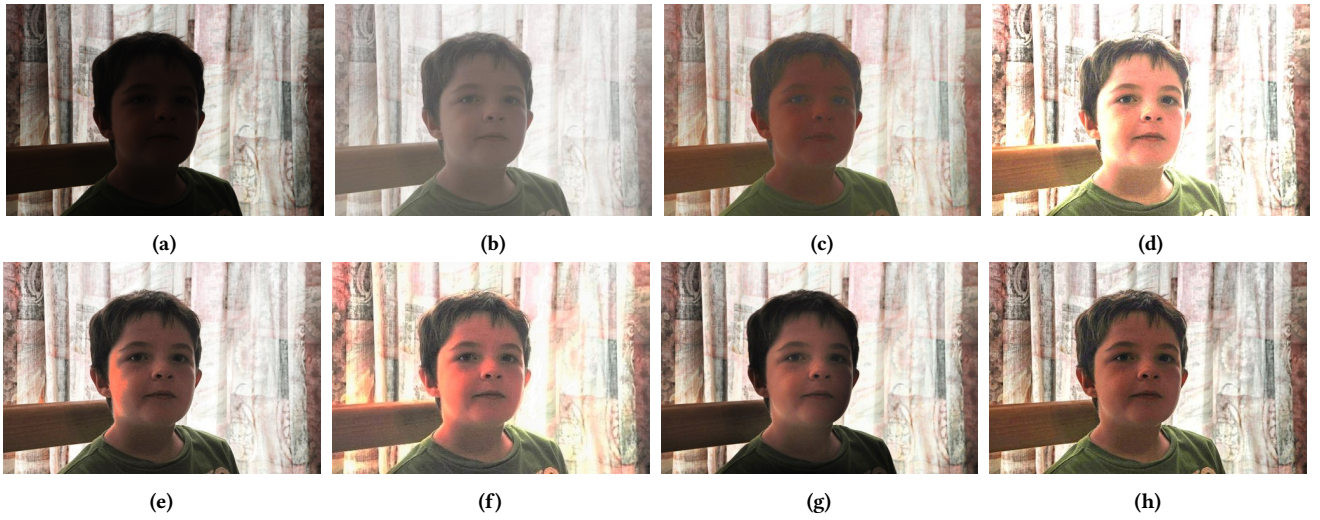


**Figure 9: Evaluation of the proposed PBS constraints.** (a) Input. (b) Gamma correction result using  $I^Y$  with  $\gamma = 0.4$ . (c) Result from the initial illumination  $S'$ . (d) Result from RTV [32] smoothed illumination. (e)-(g) are our results without the color, texture and exposure consistency constraint, respectively. (h) Our results with all the constraints.

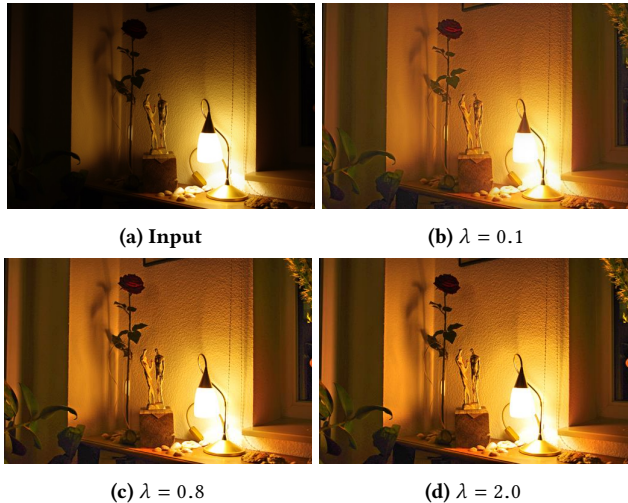


**Figure 10: Effect of varying  $\lambda$  on the result.**

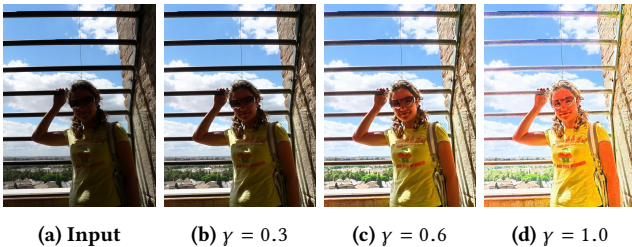


**Figure 11: Effect of varying  $\gamma$  on the result.**

## 5 CONCLUSION

In this paper, we have proposed an effective criterion, called perceptually bidirectional similarity (PBS), for enabling high-quality exposure correction of underexposed photos. The PBS reveals why

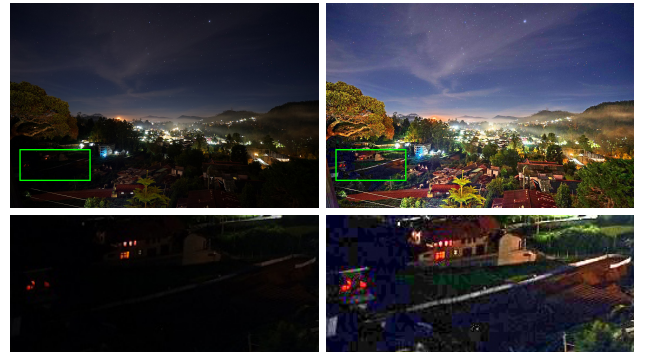


**Figure 12: Limitations.** Left: input. Right: our result.

existing methods fail to produce natural-looking results, and illustrates how we can produce results without these disturbing issues by preserving a visual similarity between the input and the output. Based on this criterion and the Retinex theory, we cast the exposure correction problem as a illumination estimation optimization, where PBS is converted into three constraints on illumination for simultaneously ensuring the color, texture and exposure consistency. We derive an ADMM based procedure for efficiently optimizing the non-convex model. Qualitative and quantitative comparisons along with the user study have demonstrated the advantage of our method over state-of-the-art methods.

## ACKNOWLEDGMENTS

This work was partially supported by the National Key Research and Development Program of China (2018YFB1004903), National Science Foundation of China (61522115, 61661130157, U1611461, 61772570), Guangdong Province Science and Technology Innovation Leading Talents (2016TX03X157), Pearl River S&T Nova Program of Guangzhou and Guangdong Natural Science Funds for Distinguished Young Scholar, the PhD Start-up Fund of Natural Science Foundation of Guangdong Province (2015A030310450).

## REFERENCES

- [1] Eric P Bennett and Leonard McMillan. 2005. Video enhancement using per-pixel virtual exposures. In *ACM Transactions on Graphics (TOG)*, Vol. 24. 845–852.
- [2] Stephen Boyd, Neal Parikh, Eric Chu, Borja Peleato, and Jonathan Eckstein. 2011. Distributed optimization and statistical learning via the alternating direction method of multipliers. *Foundations and Trends in Machine Learning* 3, 1 (2011), 1–122.
- [3] Vladimir Bychkovsky, Sylvain Paris, Eric Chan, and Frédo Durand. 2011. Learning photographic global tonal adjustment with a database of input/output image pairs. In *CVPR*. IEEE, 97–104.
- [4] Bolun Cai, Xianming Xu, Kailing Guo, Kui Jia, Bin Hu, and Dacheng Tao. 2017. A Joint Intrinsic-Extrinsic Prior Model for Retinex. In *ICCV*. 4000–4009.
- [5] Turgay Celik and Tardi Tjahjadi. 2011. Contextual and variational contrast enhancement. *IEEE Transactions on Image Processing* 20, 12 (2011), 3431–3441.
- [6] Xuan Dong, Guan Wang, Yi Pang, Weixin Li, Jiangtao Wen, Wei Meng, and Yao Lu. 2011. Fast efficient algorithm for enhancement of low lighting video. In *International Conference on Multimedia and Exposition*. IEEE, 1–6.
- [7] Xueyang Fu, Yinghao Liao, Delu Zeng, Yue Huang, Xiao-Ping Zhang, and Xinghao Ding. 2015. A probabilistic method for image enhancement with simultaneous illumination and reflectance estimation. *IEEE Transactions on Image Processing* 24, 12 (2015), 4965–4977.
- [8] Xueyang Fu, Delu Zeng, Yue Huang, Yinghao Liao, Xinghao Ding, and John Paisley. 2016. A fusion-based enhancing method for weakly illuminated images. *Signal Processing* 129 (2016), 82–96.
- [9] Xueyang Fu, Delu Zeng, Yue Huang, Xiao-Ping Zhang, and Xinghao Ding. 2016. A weighted variational model for simultaneous reflectance and illumination estimation. In *CVPR*. 2782–2790.
- [10] Yuanyuan Gao, Hai-Miao Hu, Bo Li, and Qiang Guo. 2018. Naturalness Preserved Nonuniform Illumination Estimation for Image Enhancement Based on Retinex. *IEEE Transactions on Multimedia* 20, 2 (2018), 335–344.
- [11] Rafael C. Gonzalez and Richard E. Woods. 2002. *Digital Image Processing (2nd Ed)*. Prentice Hall.
- [12] Roger Grosse, Micah K Johnson, Edward H Adelson, and William T Freeman. 2009. Ground truth dataset and baseline evaluations for intrinsic image algorithms. In *ICCV*. IEEE, 2335–2342.
- [13] Xiaojie Guo, Yu Li, and Haibin Ling. 2017. LIME: Low-Light Image Enhancement via Illumination Map Estimation. *IEEE Transactions on Image Processing* 26, 2 (2017), 982–993.
- [14] Nicolas Hautière, Jean-Philippe Tarel, Didier Aubert, and Eric Dumont. 2011. Blind contrast enhancement assessment by gradient ratioing at visible edges. *Image Analysis & Stereology* 27, 2 (2011), 87–95.
- [15] Daniel J Jobson, Zia-ur Rahman, and Glenn A Woodell. 1997. A multiscale retinex for bridging the gap between color images and the human observation of scenes. *IEEE Transactions on Image processing* 6, 7 (1997), 965–976.
- [16] Daniel J Jobson, Zia-ur Rahman, and Glenn A Woodell. 1997. Properties and performance of a center/surround retinex. *IEEE Transactions on Image Processing* 6, 3 (1997), 451–462.
- [17] Ron Kimmel, Michael Elad, Doron Shaked, Renato Keshet, and Irwin Sobel. 2003. A variational framework for retinex. *International Journal of Computer Vision* 52, 1 (2003), 7–23.
- [18] Edwin H Land. 1977. The retinex theory of color vision. *Scientific American* 237, 6 (1977), 108–129.
- [19] Chulwoo Lee, Chul Lee, and Chang-Su Kim. 2013. Contrast enhancement based on layered difference representation of 2D histograms. *IEEE Transactions on Image Processing* 22, 12 (2013), 5372–5384.
- [20] Yu Li and Michael S Brown. 2014. Single image layer separation using relative smoothness. In *CVPR*. 2752–2759.
- [21] Chih-Jen Lin. 2007. Projected gradient methods for nonnegative matrix factorization. *Neural computation* 19, 10 (2007), 2756–2779.
- [22] Kin Gwn Lore, Adedotun Akintayo, and Soumik Sarkar. 2017. LLNet: A deep autoencoder approach to natural low-light image enhancement. *Pattern Recognition* 61 (2017), 650–662.
- [23] Kede Ma, Kai Zeng, and Zhou Wang. 2015. Perceptual quality assessment for multi-exposure image fusion. *IEEE Transactions on Image Processing* 24, 11 (2015), 3345–3356.
- [24] Tom Mertens, Jan Kautz, and Frank Van Reeth. 2009. Exposure fusion: A simple and practical alternative to high dynamic range photography. In *Computer Graphics Forum*, Vol. 28. Wiley Online Library, 161–171.
- [25] Michael K Ng and Wei Wang. 2011. A total variation model for Retinex. *SIAM Journal on Imaging Sciences* 4, 1 (2011), 345–365.
- [26] Stephen M Pizer, E Philip Amburn, John D Austin, Robert Cromartie, Ari Geselowitz, Trey Greer, Bart ter Haar Romeny, John B Zimmerman, and Karel Zuiderveld. 1987. Adaptive histogram equalization and its variations. *Computer vision, graphics, and image processing* 39, 3 (1987), 355–368.
- [27] Li Shen and Chuohao Yeo. 2011. Intrinsic images decomposition using a local and global sparse representation of reflectance. In *CVPR*. IEEE, 697–704.
- [28] Liang Shen, Zihao Yue, Fan Feng, Quan Chen, Shihao Liu, and Jie Ma. 2017. MSR-net: Low-light Image Enhancement Using Deep Convolutional Network. *arXiv preprint arXiv:1711.02488* (2017).
- [29] Carlo Tomasi and Roberto Manduchi. 1998. Bilateral filtering for gray and color images. In *ICCV*. IEEE, 839–846.
- [30] Liqian Wang, Liang Xiao, Hongyi Liu, and Zhihui Wei. 2014. Variational Bayesian method for retinex. *IEEE Transactions on Image Processing* 23, 8 (2014), 3381–3396.
- [31] Shuhang Wang, Jin Zheng, Hai-Miao Hu, and Bo Li. 2013. Naturalness preserved enhancement algorithm for non-uniform illumination images. *IEEE Transactions on Image Processing* 22, 9 (2013), 3538–3548.
- [32] Li Xu, Qiong Yan, Yang Xia, and Jiaya Jia. 2012. Structure extraction from texture via relative total variation. *ACM Transactions on Graphics (TOG)* 31, 6 (2012), 139.
- [33] Zhengmao Ye, Habib Mohamadian, and Yongmao Ye. 2007. Discrete entropy and relative entropy study on nonlinear clustering of underwater and aerial images. In *International Conference on Control Applications*. IEEE, 313–318.
- [34] Li Yuan and Jian Sun. 2012. Automatic exposure correction of consumer photographs. In *ECCV*. Springer, 771–785.
- [35] Kai Zeng, Kede Ma, Rania Hassoun, and Zhou Wang. 2014. Perceptual evaluation of multi-exposure image fusion algorithms. In *International Workshop on Quality of Multimedia Experience (QoMEX)*. IEEE, 7–12.
- [36] Qing Zhang, Yongwei Nie, Ling Zhang, and Chunxia Xiao. 2016. Underexposed video enhancement via perception-driven progressive fusion. *IEEE Transactions on Visualization and Computer Graphics* 22, 6 (2016), 1773–1785.
- [37] Qi Zhao, Ping Tan, Qiang Dai, Li Shen, Enhua Wu, and Stephen Lin. 2012. A closed-form solution to retinex with nonlocal texture constraints. *IEEE Transactions on Pattern Analysis and Machine Intelligence* 34, 7 (2012), 1437–1444.
- [38] Qing-Nan Zhao, Ting-Zhu Huang, Xi-Le Zhao, Tian-Hui Ma, and Ming-Hui Cheng. 2017. A Convex Optimization Model and Algorithm for Retinex. *Mathematical Problems in Engineering* 2017 (2017).
- [39] Karel Zuiderveld. 1994. Contrast limited adaptive histogram equalization. In *Graphics gems IV*. 474–485.